The impact of wavelet estimation in 4D inversion — an offshore Brazil case study

Ekaterina Kneller[1*], Ulisses Correia[1], Jean-Philippe Coulon[1], Laryssa Oliveira[1], Paulo de Oliveira Maciel Junior[2] and Wilson Lisboa Ramos Filho[2] demonstrate how wavelet estimation in 4D inversion in a post-salt turbidite reservoir in the Campos Basin can lead to significant uplift in the mapping of 4D anomalies.

Introduction

The development and production of post-salt turbidite reservoirs frequently present a challenge. One effective tool for understanding fluids and pressure effects in reservoirs is 4D global inversion. This tool can be used to obtain changes in elastic properties over time, helping to reduce uncertainty in mapping 4D anomalies. The 4D global inversion workflow is a multistage process that includes seismic data preconditioning, wavelet estimation, low-frequency model building, 3D inversion, and finally a 4D global inversion. This inversion algorithm benefits from an iterative and non-linear optimization process that greatly improves the 4D interpretation. In this work, focusing on a post-salt turbidite reservoir in the Campos Basin, offshore Brazil, we show how this process can help to better understand the 4D seismic data, bringing a significant uplift in the quality of the mapping of the 4D anomalies. Special attention was paid to the wavelet estimation process, which played a significant role in this case study. The 4D inversion results helped in the decision-making process for selecting new well locations in the study area. The objective of this work is to demonstrate the benefits of assessing the impact of the inversion parameters, particularly wavelets, on 4D interpretation.

Geological setting

The field is located in the Campos Basin, in the southeastern region of the Brazilian continental margin. A 6 km wide channel represents its external geometry, elongated in the NW-SE direction. The production zone comprises Eocene turbidite sandstone reservoirs deposited in a deep marine environment. The reservoirs have good porosity (29% on average), good absolute permeability (2500 mD on average), and a large active aquifer, which is efficient at maintaining reservoir pressure. The oil gravity is 19° API.

Although the external geometry of the reservoir is well resolved using the available 3D seismic data, internal details of the oil zone are very difficult to observe owing to the impact of the fluid (oil) in the seismic signal.

4D survey design and seismic processing

This study relates to a time-lapse (4D) seismic processing project performed in 2018/2019, which benefited from all the latest advanced processing technologies available in the industry at the time to enhance reservoir monitoring and characterization. The baseline survey was acquired in 2005 and the monitor survey in 2018. Both surveys deployed streamer vessels towing 6 km long cables, 50 m apart, with 480 channels in each cable. A configuration of two sources spaced 25 m apart was used. The main objective was to evaluate the 4D seismic signal in post-salt reservoirs. Processing efforts focused on preserving data amplitude and removing source- and receiver-related ghosts. A set of pre-stack depth migration (PSDM) imaging techniques, as well as state-of-the-art time-lag full waveform inversion (TL-FWI) and least-squares (LS) migration technologies, were also applied.

Furthermore, to improve the repeatability between surveys, seismic conditioning processes were performed prior to the 4D seismic inversion study. These included random noise filtering, and structurally consistent filtering, 4D warping and residual time-misalignment correction with very small time shifts which do not impact the frequency content.

Global 4D inversion

The main purpose of 4D inversion is to derive a model of the changes in the elastic properties of the reservoir from the seismic amplitude variations between vintages. The impedances characterize the interval properties of the rocks, while the reflectivity characterizes the contrasts between intervals. The result of 4D inversion is the P-Impedance (Ip) volume for the base and monitor surveys and the analysis is performed through interpretation of the Ip Ratio calculated using the following equation:

$$\text{Ip Ratio} = 100*(\text{Ip\_moni} - \text{Ip\_base})/\text{Ip\_base}.$$

The 4D inversion workflow is a multistep process including:

1. Well-to-seismic calibration and wavelet estimation,
2. Stratigraphic model building,
3. Initial low-frequency model,
4. 3D inversion,
5. 4D inversion as an iterative process with parameter optimization.

[1] CGG | [2] Petrobras
* Corresponding author, E-mail: ekaterina.kneller@CGG.com
DOI: 10.3997/1365-2397.fb2021082

1. Well-to-seismic calibration and wavelet estimation are key steps in the inversion process because they link seismic amplitude and reflectivity derived from elastic properties. Table 1 summarizes the workflow used for wavelet estimation. All the wavelets were extracted from the near partial stack (8 degrees). The initial guess is usually based on a zero-phase statistical wavelet (Edgar and van der Baan, 2011). Wavelet WV1 was estimated for a time window of 1 second in the vicinity of three well locations, which were sufficiently representative of the entire volume (Figure 1). The jittering of the frequency spectrum can be stabilized by adding more traces or smoothing the frequency spectra (Figure 1). The smoothing effect with the use of a 3 Hz moving window is demonstrated by wavelet WV2 (WV1 with the smoothing applied). Based on a visual evaluation, the smoothing effect is stronger where the spectrum is 'steeper' – the curves diverge between 0 and 7 Hz (Figure 1).

Once the statistical wavelet has been obtained, the well-to-seismic tie can be performed and refined. We recommend applying minimal stretch and squeeze editing to the time-depth curve, respecting the check-shots or integrated sonic logs. A deterministic wavelet can then be estimated at each well location with the amplitude and phase spectra that provide the maximum cross-correlation between the seismic and synthetic traces. Figure 2A shows the result of wavelet estimation in three wells, W001, W004, and W006. When the deterministic wavelets are being extracted, the use of constraints (taper, smoothing, averaging between wells) becomes important, since every mismatch between seismic and well reflectivity impacts the wavelets (Figure 2A). Usually, at this stage, some wells are excluded from the wavelet estimation process – as is the case for well W006, which was excluded from the analysis owing to a 'noisy' individual wavelet, which is an indication of the uncertainty in its well-to-seismic calibration. As mentioned above, the extraction process requires some constraints – we applied smoothing of phase spectra in a 3 Hz window (Figure 2B). The phase was computed in the 4 to 48 Hz frequency interval and extrapolated out of this interval. Only traces with correlation coefficients greater than 0.6 were used in the extraction.

In Figure 3 we observe two main differences between statistical wavelet WV2 and multi-well wavelet WV4. Firstly, WV2 has higher amplitude high-frequency content (20-80 Hz) and, secondly, WV2 has lower amplitude low-frequency (0-10 Hz) content. This difference in low frequency content can be interpreted as a bias introduced by the use of a short vertical time window for the wavelet extraction, owing to the limited interval where either the logs are available and/or the match between seismic and synthetic is sufficiently good. To attenuate the secondary lobes that may still be observed on the wavelets in the time domain and that can be interpreted as noise, we decided to use stronger constraints. For example, WV5 was extracted in the same way as WV4 but using a 10 Hz smoothing window to obtain a smoother phase and amplitude spectra. Figure 2C shows the individual wavelets and Figure 3 shows the multi-well wavelet for comparison. Increasing the smoothing attenuates secondary lobes and noise. Unfortunately, it also has a significant impact on the width of the central lobe, which may affect the vertical resolution, and the low frequencies (0-5 Hz), which may introduce a bias compared to the WV4 (red) and the WV5 (blue) spectra (Figure 3). We generated three wavelet versions for subsequent inversion tests: WV2 – the statistical wavelet with the 3 Hz smoothing window applied, WV4 – the constrained well wavelet, and WV5 – the more constrained well wavelet, which contains fewer sidelobes and noise. Despite observing the constant component in wavelets WV4 and WV5, these wavelets were used in the inversion tests to demonstrate the possible impact on the inversion result.

2. Stratigraphic model construction is an important stage in the workflow because the inversion used is layer-based – the average thickness of microlayers and the geometry of the layering must be optimized depending on the seismic resolution and stratigraphic context.

3. Initial low-frequency model building is an essential part of 3D inversion to obtain a reliable absolute elastic model from the inversion process using five partial angle stacks

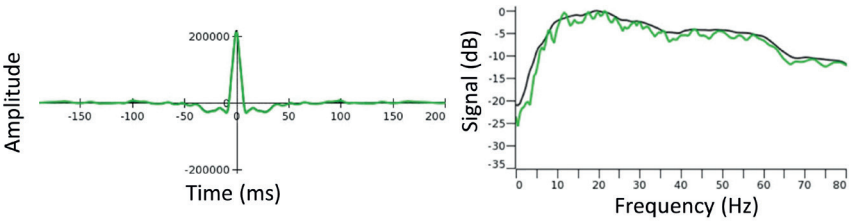

Figure 1 WV1 and WV2. Statistical wavelets and amplitude spectra without (green, WV1) and with (black, WV2) smoothing using a 3 Hz moving window.

Short description	Parameters	Name	Complementary Low-Pass Filter
First guess	Statistical wavelets	WV1	3-12 Hz
Statistical 'good looking'	Smooth 3 Hz applied to the WV1	WV2	3-12 Hz
'Raw' well wavelets	Well wavelets without constraints	WV3	
Constrained well wavelets	Well wavelets with soft constraints	WV4	1-8 Hz
Overconstrained well wavelets	Well wavelets with harsh constraints	WV5	0-6 Hz

Table 1 Wavelet extraction workflow. All the wavelets were extracted from the near partial stack (8 degrees).

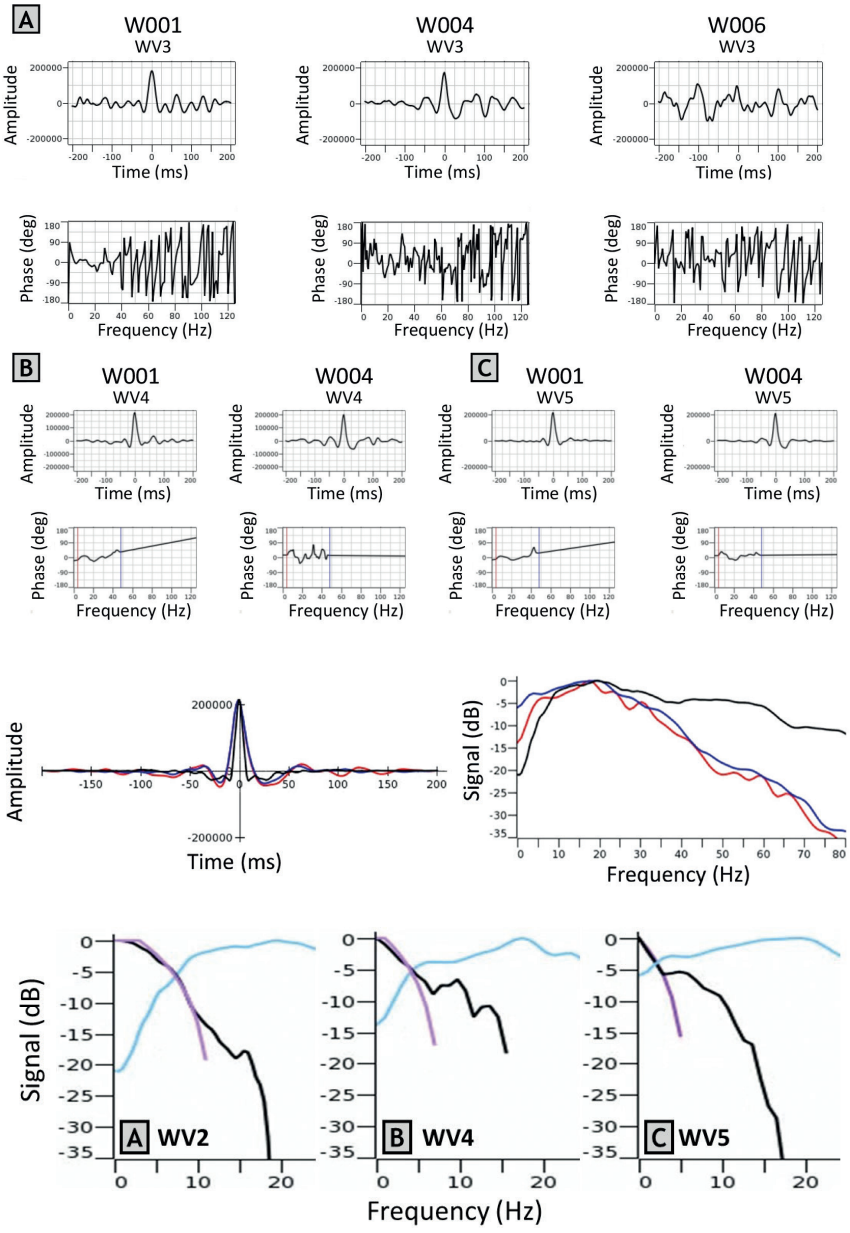

Figure 2 A).WV3. Wavelets are estimated with well data for wells W001, W004 and W006 without using any constraint or stabilization. B). WV4. Wavelets are estimated with well data with 3 Hz smoothing. C). WV5. Wavelets are estimated with well data with 10 Hz smoothing.

Figure 3 Comparison of wavelets. WV2 statistical wavelet (black), WV4 constrained multi-well wavelet (red), and strongly constrained multi-well wavelet WV5 (blue).

Figure 4 Low-pass filters were designed for the three wavelets. The blue curve is a spectrum of the wavelet, the black curve is the calculated complementary filter, and the magenta curve is the low-pass ramp defined by two frequency values matching the complementary black spectra. A) for wavelet WV2 – low pass 3-12 Hz, B) for WV4 – low pass 1-8 Hz, C) for WV5 – low pass 0-6 Hz.

covering incidence angles of up to 36 degrees. Considering the band-limited seismic data, the main objective is to fill the gap in the low-frequency range that is not present in the seismic data. Figure 4 shows the low-pass complementary filters designed for the wavelets. The statistical wavelet WV2 requires a 3-12 Hz low-pass filter for the initial model. The constrained multi-well wavelet WV4 requires a 1-8 Hz low-pass filter for the initial model. The additionally smoothed wavelet WV5 requires a 0-6 Hz low-pass filter for the initial model. Adding the wells and the smoothing 'boosts' low frequencies in the wavelets and means, as a result, that the initial model requires a narrower frequency corridor. The properties required in the inversion were propagated in the stratigraphic model with collocated co-kriging using the seismic velocity as a second variable.

4. 3D Inversion as described by Coulon et al. (2006) is part of the 4D inversion workflow because it provides the initial model for the 4D inversion.

Using the three different wavelets (WV2, WV4, and WV5) and their corresponding low-frequency models, based on the values shown in Figure 4, 3D inversion runs were performed. Figure 5 shows a comparison section through the acoustic impedance volumes. The inversion with the WV2 statistical wavelet (A) demonstrates the strongest low-frequency content compared to the inversion using the WV4 (B) and WV5 (C) well wavelets. The accuracy of the 3D inversion can be numerically evaluated through an analysis of the match to the well log values – this is one of the main decision-making criteria in the inversion parameter optimization process. The three inversion tests demonstrate similar correlation values (around 0.7) between the upscaled impedance logs and inversion results, so, based on this, none of the tests can be judged to be better than the others. The quality of the 3D inversion result based on the correlation values alone cannot be used as a criterion for the wavelet choice.

5. Further analysis was performed through a **global 4D inversion** method described by Lafet et al. (2008) using the workflow

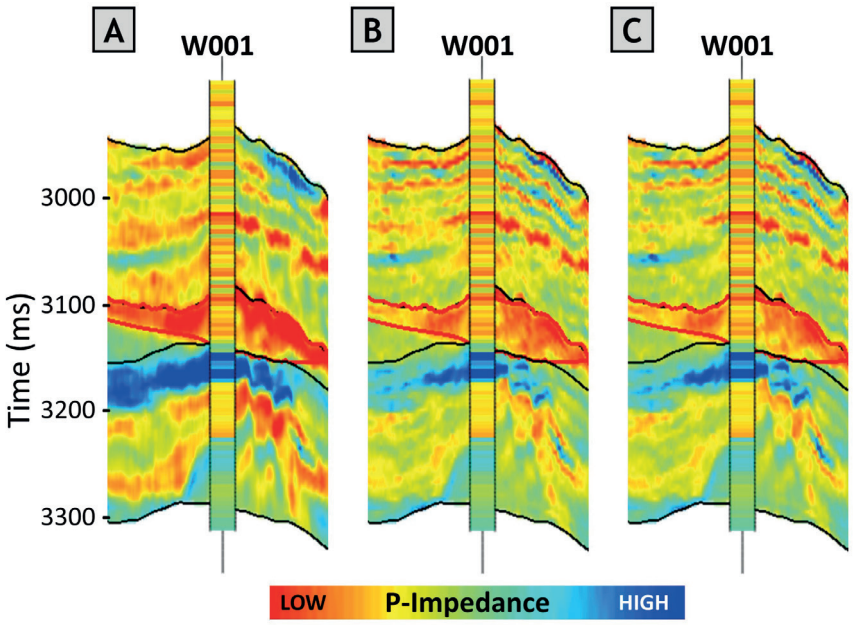

Figure 5 3D inversion results intersecting well W001 A) with statistical wavelet WV2 and initial 3-12 Hz model, B) with constrained multi-well wavelet WV4 and initial 1-8 Hz model, C) with strongly constrained multi-well wavelet WV5 and initial 0-6 Hz model.

shown in Figure 6. As for the 3D inversion process, 4D inversion minimizes a cost function using a Simulated Annealing procedure. However, it is adapted to the multi-vintage setting and allows user control over the level of 4D coupling between inverted elastic attributes. The objective is to find a global solution that simultaneously optimizes the match between the input angle stacks for all vintages and the corresponding synthetics. Time-lapse coupling is achieved by restricting the range of the perturbations between successive surveys according to user-specified constraints, based on physical knowledge of the 4D changes. This makes it possible to reduce the inversion non-uniqueness and limit the solution space. These user-defined bounds integrate several pieces of information summarizing the degree of confidence in the initial model, the reliability of the rock-physics information linking successive surveys, the magnitude of the 4D signal and other geological interpretation constraints.

In this study, we only show the acoustic part of the 4D inversion as it is the main variable for analysing the 4D signature in the context of the field, with a dominant fluid change response, no temperature effect, no compaction, no strong pressure change, and no salinity issues. The challenge of 4D inversion parametrization lies in the absence of direct numerical quality controls (i.e, matching with well logs as in 3D inversion), which would allow informed decision making about the choice of parameter values. In this study, and considering the information available, we decided to start from an identical initial elastic model for the different vintages (no initial 4D difference was introduced). This initial model is based on the results obtained from a preliminary 3D inversion of the Base vintage. Out of curiosity to see the impact of the estimated wavelets, the 4D inversion test was performed with the three different wavelets. Test A is a 4D inversion with statistical WV2, test B uses the constrained WV4 and test C uses the strongly constrained WV5. Figure 7 shows the sections through the Ip Ratio volumes from these 4D inversion tests.

The Ip Ratio extracted from inversion A with statistical wavelet WV2 contains a lower-amplitude signal outside the reservoir compared to the Ip Ratio from inversion tests B and C which

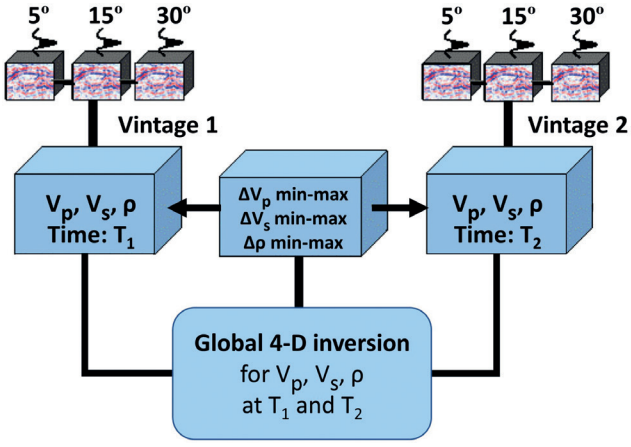

Figure 6 Global 4D inversion of multiple seismic vintages and angle stacks with 4D corridor constraints for coupling inverted attributes between successive surveys. A wavelet is an input for each partial stack (modified from Lafet et al., 2008).

uses the well wavelets WV4 and WV5. The main 4D anomalies – softening (red) and hardening (blue) – are less prominent against the increasing 4D noise in tests B and C. The strong 4D response outside the reservoir interval (defined by the black horizons) – in Figure 7 – prompted us to check the seismic data more carefully and we found a difference between the frequency content of the Base and Monitor in the 0-10 Hz interval (Figure 8). This observation inspired a series of tests with different wavelets for the Base and Monitor in the global 4D inversion. In the initial tests, the same wavelets that were created for the Base vintage were also used for the Monitor vintage even though this could potentially introduce more bias in the results due to the absence of any production effects in the well logs. Tests D, E, and F in Figure 7 correspond to the inversion with different wavelets for the Base and Monitor. By using different wavelets it is possible to significantly attenuate the 4D noise outside the reservoir because they help to compensate for the difference in the bandwidth of Base and Monitor. When the statistical wavelets are used – comparing tests A and D – we can see the significant uplift in the amplitude of the signal compared

to the noise level. The 4D noise tends to decrease also for tests E and F compared to tests B and C respectively, but at the same time, in other locations, noise is introduced by the wavelet difference. This is explained by the wavelet estimation bias when using well data in a short estimation window, in addition to the impact of the constraints and smoothing. Both these factors impact mostly the low-frequency part of the spectra where the difference between Base and Monitor was observed. To evaluate the 4D inversion tests quantitatively, the ratio of 4D Energy inside and outside the reservoir was used as a metric. First, for every test, we extracted the map of the energy for the reservoir interval. Then, both Top and Base horizons were shifted 150 ms below to obtain a similar interval outside the reservoir and the energy was estimated there. These values of energy were calculated using Impedance Ratio volumes and Table 2 shows the average values for each test in the representative rectangular area consisting of 230,000 traces. Test D, 4D inversion with the use of statistical wavelets extracted separately for the Base and Monitor, was selected as the best result based on the 4D Energy ratio and was used in the subsequent analysis. The energy inside the reservoir for this test is 5.48 times stronger than the energy outside the reservoir, while in other tests this metric has lower values – it decreases drastically when we analyse tests B, C, E, and F which use the well wavelets. The tests using the different wavelets for the Base and Monitor (D, E, F) have higher values of the metric compared to the tests with the same wavelets for the Base and Monitor (A, B, C). This analysis shows that the bias in wavelet estimation can have a strong negative impact on the 4D inversion result adding 4D noise to results and can be unidentifiable in the preceding 3D inversion tests.

Interpretation of results

The whole 4D inversion parametrization process required close interaction between the geophysicists and the interpreters because, unlike 3D inversion, no detailed quantitative quality control analysis is available. All impedance variations observed in the 4D inversion results are directly linked to the effects of field production, and require validation by a field specialist. In the light of that, we based all our final geological interpretation work on the best test we obtained from the sensitivity analysis we made - test D. We should also mention that the interpretation itself is a fundamental component of this whole inversion process.

4D inversion test	Energy inside reservoir	Energy outside reservoir	Ratio of Energy inres/ outres
A	2.24	0.47	4.77
B	1.81	0.70	2.59
C	1.96	0.72	2.72
D	2.41	0.44	5.48
E	1.74	0.69	2.52
F	1.81	1.71	1.06

Table 2 The ratio of energy inside and outside the reservoir for ratio impedance in 4D inversion tests.

Currently, the drainage strategy for this reservoir consists of four horizontal producing wells positioned at the top of the channel complex away from the oil-water contact level.

A large aquifer maintains the effective pressure in the reservoir close to its original value, but two injection wells, which are also horizontal, and positioned in the northern portion of the field, inject water to help to maintain pressure and guide the hydrocarbon flow. However, the low efficiency of the injecting wells during the period between the seismic surveys resulted in the formation of a gas cap just above the production wells in the upper part of the structure.

The producer wells started operating between 2008 and 2015, while the injectors have been operating since 2011. The 4D seismic analysis between 2005 and 2018 is therefore suitable for evaluating the dynamic behaviour of the reservoir. The pressure regime is globally stable and only a few isolated compartments may be relevant.

For this reservoir, oil sands are typically of lower impedance than the shales, resulting in a negative seismic amplitude response at the top of the reservoir and positive response at the base (Figure 9D). The 3D acoustic impedance section shows

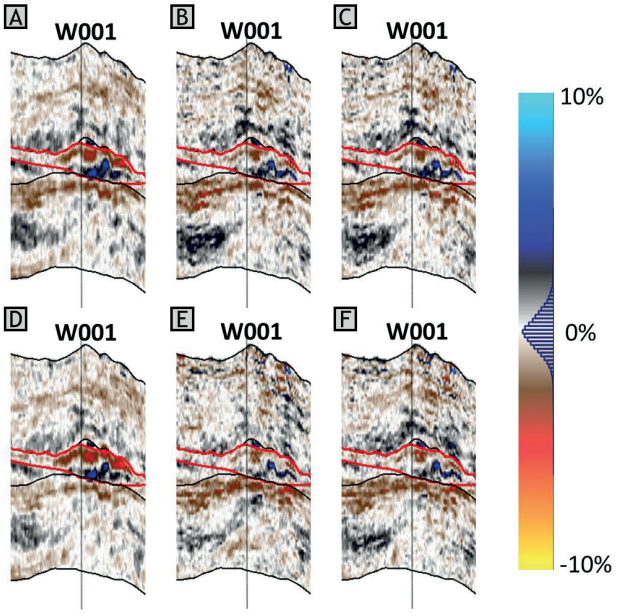

Figure 7 4D inversion test results. A) Common WV2 wavelet for Base and Monitor B) Common WV4 wavelet for Base and Monitor C) Common WV5 wavelet for Base and Monitor D) Different WV2 wavelets for Base and Monitor E) Different wavelets for Base and Monitor, WV4, F) Different wavelets for Base and Monitor, WV5. The black horizons define the top and the base of the reservoir formation interval, and the red horizons limit the top of the oil leg, without a gas cap in the vicinity of the well, and the base of the oil leg merged with the oil-water contact.

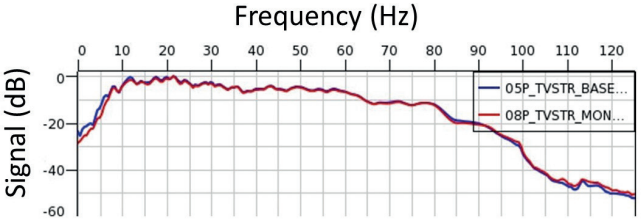

Figure 8 Frequency spectra of the Base and Monitor seismic datasets showing a difference in the 0-7 Hz range.

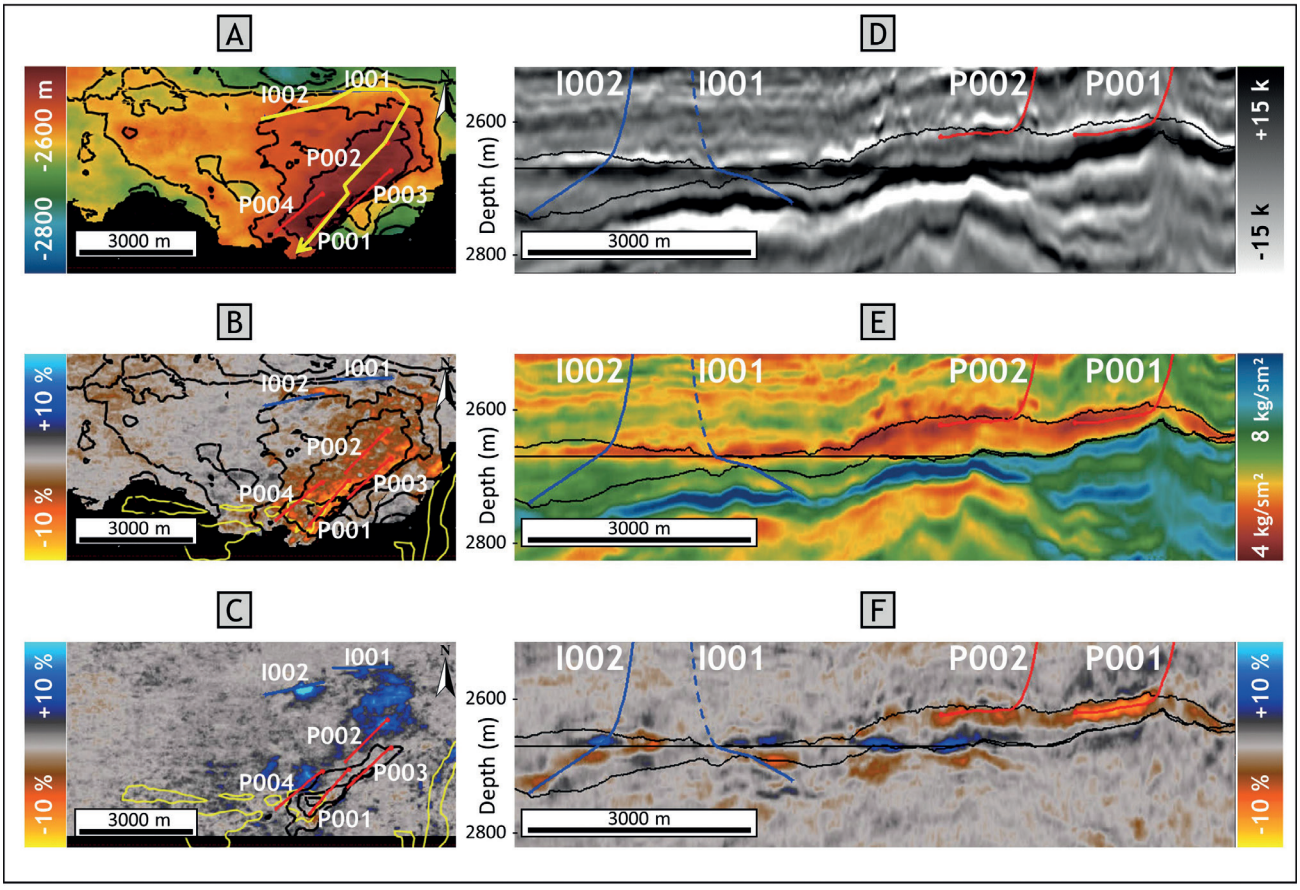

Figure 9 4D geophysical interpretation and integration with reservoir management. A) Reservoir top depth map. B) Maximum negative values of the relative acoustic impedance ratio, indicating impedance decreases, in a 10 m layer at the top of the reservoir. C) Maximum positive values of the relative acoustic impedance ratio, indicating impedance increases, in a 25 m layer at the base of the reservoir. D) 3D seismic amplitude of the Base. E) 3D acoustic impedance from 3D seismic inversion of the Base. F) 4D inversion acoustic impedance ratio. In map A, the yellow line represents the arbitrary line location through selected wells for the sections on the right. In maps B and C, the yellow polygons represent the outline of regions with low 4D seismic repeatability (high NRMS above the reservoir) due to surface obstructions. In sections D, E, and F the black lines are the top and base reservoir, and the oil-water contact. In both map and section views, the injectors are in blue (I001, I002) and the producers are in red (P001, P002, P003, P004).

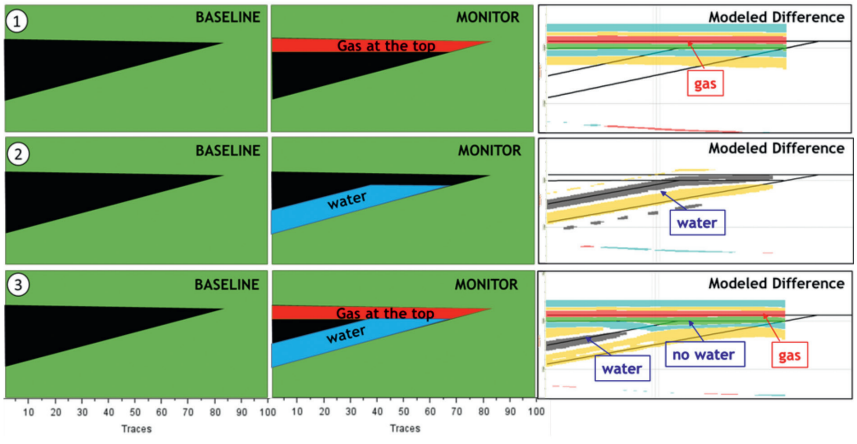

Figure 10 Illustrative 4D seismic amplitude modelling for different wedge model scenarios: gas saturation increases at the top (1), water saturation increases at the base (2), and both simultaneously (3).

the strong seismic response to the fluid content, indicating the oil-water contact (Figure 9E).

As a result of the high-quality data, it was possible to identify anomalies mainly related to changes in fluid saturation in the 4D seismic response. In terms of other reservoir property changes which could result in a 4D seismic response, the effects of temperature and salinity can be ignored and the pressure drop is also small, but significantly, initial pressure was just above the bubble point.

The softening anomalies at the top of the reservoir (Figures 9B and 9F) are related to an increase in gas saturation. Because of the depletion history of the field and the temporary increase in the produced gas-oil ratio, the most likely interpretation is that pressure has declined below the bubble point, causing gas to break out of the solution. Therefore, this gas that is out of solution migrates upwards to the top of the reservoir and forms a secondary gas cap. In Figure 9F we can see differences in the intensities of

this softening effect, which may be related to lower depletion and gas saturation observed in well P002 when compared to producer P001. Through interpretation of this volume, we can evaluate different reliability scenarios for the continuity of the anomaly corresponding to the gas layer, at the time of the Monitor survey. Using 4D seismic data to gain insight into the gas distribution and understand its cause played a significant role in field management.

In addition to the 4D anomalies related to the presence of gas, there are also anomalies associated with the presence of water in the lower portions of the oil zone. In Figures 9C and 9F, blue areas indicate increases in impedance, which is the result of water replacing oil. Furthermore, the limit of the anomaly on the eastern flank is conformable with structure and movement in the oil-water contact. These changes can be observed around injection wells I001 and I002 (Figure 9C, north), where the water was injected into a thin oil zone and shifted the oil-water contact towards the producing wells on top of the structure (Figure 9A, dark red area). The advancement of water, especially from the aquifer, is observed where the water saturation increases near the producing wells yielding an impedance increase (hardening anomaly) in the blue areas (Figure 9C and 9F).

In Figure 9F, on the right of injector well I002 (also in Figure 9B), there is a small region with a local impedance decrease (negative values, softening anomaly) interpreted as an overpressure caused by injection in a locally compartmentalized region. Although there is a discontinuity in the top of the reservoir along the section between injecting wells I001 and I002, the compartmentalization could not be identified using only the 3D data (Figures 9D and 9E).

The increases in acoustic impedance observed in Figure 9F close to the oil-water contact denote the rising of this surface towards the producing region. However, it is interesting to note that below well P001 there is no hardening effect like the one observed below well P002, even though production from these wells showed a similar increase in water saturation between the Base and Monitor surveys. According to a fluid substitution modelling based on a representative reservoir well (Figure 10), the 4D data was not expected to be of sufficient resolution to simultaneously detect changes related to the softening at the top of the reservoir and a hardening just below well P001. On the other hand, below producing well P002, where the reservoir is thicker, it is possible to detect the softening and hardening anomalies associated with increases in gas and water saturation, respectively. In addition to the difference in reservoir thickness, the observed difference in these anomalies may also be related to less gas saturation at the top of the structure at well P002, as previously stated.

The results for this reservoir show significant movement of the oil-water contact on the northern and eastern sides of the field. On the other hand, there is no apparent water movement in the central part between wells I002 and P002, suggesting there may be additional drilling opportunities there.

Conclusions

In this study, we presented a detailed description of 4D global inversion, paying particular attention to wavelet extraction, which helped us to understand its impact on the 4D interpretation. In this way, it was possible to minimize inversion artifacts and improve confidence in the results. We have shown the merits of a stepwise approach in parametrizing the 4D inversion, particularly for handling the wavelets. We also demonstrate that the consistent and highly reliable 4D results we obtained, coupled with a thorough geological interpretation, enabled us to achieve a better understanding of the dynamic behaviour of the turbidite sandstone reservoir.

Acknowledgments

The authors would like to thank Petrobras and CGG for permission to publish this article. They would also like to thank Vitor Mello, from Petrobras, for his help with Figure 10 of this article that greatly supported the discussion in the interpretation of results.

References

Coulon, J.P., Lafet Y., Deschizeaux, B., Doyen, P.M. and Duboz, P. [2006]. Stratigraphic elastic inversion for seismic lithology discrimination in a turbiditic reservoir, SEG Annual Meeting, Expanded Abstracts, 2092-2096, New Orleans, US.

Edgar, J.A. and van der Baan, M. [2011]. How reliable is statistical wavelet estimation? Geophysics, **76**(4), July-August 2011; P. V59-V68, 11 figs. 10.1190/1.3587220.

Lafet, Y., Roure, B., Doyen, P.M., Bornard, R. and Buran, H. [2008]. Global 4-D seismic inversion and fluid prediction. 70th EAGE Conference & Exhibition, Rome, Italy, 9-12 June 2008.